

W. Renhart / K. Hollaus / C. Magele / G. Matzenauer

# Computation of a Bluetooth Antenna using FEM

## Abstract

Antennas using the Bluetooth - technology are of global acceptance and hence are widespread in use. In this paper the numerical simulations of a standard antenna using a dedicated FEM-based program package are described. With the FE-method the environment of the antenna can be modeled conveniently. It is very common to feed the antenna via a USB-plug. So, the main influence of the notebook casing is investigated and the changes in the radiation patterns will be reported.

**keywords** Bluetooth, finite elements, ground dependent antenna, WLAN

## Introduction

Modern wireless connections between computers and peripheral equipment operate in Bluetooth technology. Bluetooth is defined for short distance communications and became a standard. The main requirements are low power radiation at low cost devices. For industrial, scientific and medical (ISM) applications, the frequency runs between 2.4 and 2.485 GHz.

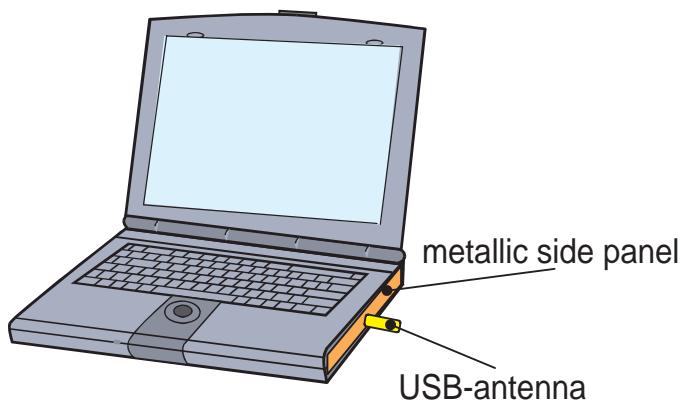


Figure 1: USB-plugged antenna with environment.

Fig. 1 shows a general arrangement, containing a PC-notebook and a USB-antenna. The metallic side panel indicated is a part of the notebook case, where

several USB connectors may be mounted. In case a Bluetooth antenna is plugged in, this side panel operates like a reflector so that a significant change in the radiation pattern is expected. The appropriate characteristics will be compared. The typical class - II radiator with a range up to 10 meters uses 2.5 mW of power. Hence, the influence on human tissue within the radiation range mentioned may be negligible.

The smallness of this kind of antennas is a fundamental demand. Hence, such antennas are manufactured simply with double-sided printed circuit boards (PCB's). In so called ground dependent antenna one side of the PCB operates as ground and the opposite side contains a standard antenna structure, e.g. meander lines or F-forms. Fig. 2 shows the structure of the standard antenna under investigation.

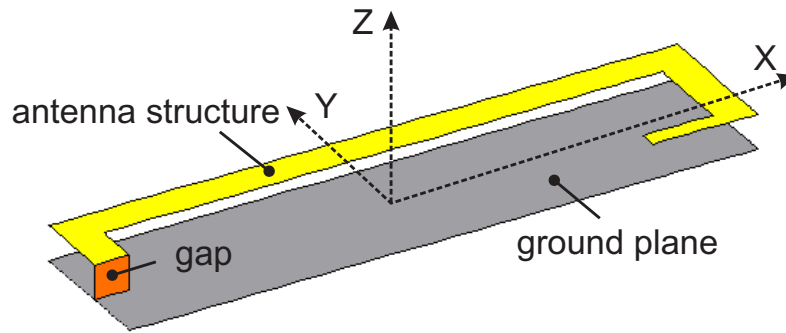


Figure 2: Geometry of the Bluetooth antenna under investigation.

## Numerical Model

With the aid of a Finite Element package, based on the well known standard  $\vec{A}v$  - formulation [0], the numerical investigations have been carried out. Using the potentials  $\vec{A}$  and  $v$  the field intensities for timeharmonic variations can be expressed by

$$\vec{E} = -j\omega\vec{A} - j\omega\nabla v \quad (1)$$

$$\vec{H} = [\nu]\nabla \times \vec{A}. \quad (2)$$

$[\nu]$  represents the magnetic reluctivity. In order to consider the displacement current density in the formulation as well, the conductivity has been made a

complex quantity. Harmonic time lapses assumed Ampere's Law can be written in the form

$$\nabla \times \vec{H} = \sigma \vec{E} + \epsilon \frac{\partial \vec{E}}{\partial t} = \underline{\sigma}_c \vec{E} \quad (3)$$

with

$$\underline{\sigma}_c \vec{E} = (\sigma + j\omega\epsilon) \vec{E}. \quad (4)$$

The real part of  $\underline{\sigma}_c$  represents the physical conductivity  $\sigma$  whereas the imaginary part includes the displacement current density. Therewith, lossy and permittive materials like human tissue may be considered as well. The FE-mesh truncation has been realized by applying perfectly matched layers, as recommended, e.g. in [0]. To compute the antenna radiation pattern for the various configurations, the vectorial Huygens principle [0] has been used. For the sake of reliability the results have been compared to solutions obtained with a dedicated FDTD-package [0].

In the FE-model, the antenna is modeled with the aid of boundary conditions. Along the grounded plane as well as along the antenna structure the electric scalar  $v$  and the tangential of  $\vec{A}$  have been enforced to be zero. This allows the displacement current density to appear in normal direction to the antenna surface, only. Along the antenna gap the tangential of  $\vec{A}$  has been prescribed and the electric scalar  $v$  has been set to zero. From (1) follows

$$\vec{E} \cdot \vec{e}_z \Delta z = -j\omega \vec{A} \cdot \vec{e}_z \Delta z = -j\omega A_z \Delta z = -U_0. \quad (5)$$

$\Delta z$  represents the gap width where the electric voltage  $U_0$  is impressed and  $\vec{e}_z$  is the unit vector in z-direction, corresponding to the co-ordinate system shown in Fig. 2.

## Numerical results

The simulated antenna of  $\frac{\lambda}{4}$ -type operates at a frequency of 2.4 GHz and the gap width  $\Delta z$  amounts 1 mm. According to the definitions in [0] the directivity for the various components of  $\vec{E}$  have been computed by

$$D_\phi(\phi, \Theta) = 2\pi \frac{|E_\phi(\phi, \Theta)|^2}{2\eta_0 P}, \quad (6)$$

$$D_\Theta(\phi, \Theta) = 2\pi \frac{|E_\Theta(\phi, \Theta)|^2}{2\eta_0 P}. \quad (7)$$

In the equations above spherical polar co-ordinates with the azimuthal angle  $\Phi$  and the polar angle  $\Theta$  have been used.  $\eta_0$  is the characteristic impedance of free space and  $P$  presents the power radiated in the far field.

## A. FEM and FDTD results in comparison

In order to gain reliability in the model developed, especially to ensure a correct choice of the PML-parameters, a FEM-based as well as a FDTD-based computation have been carried out. For this the USB-antenna without any environmental object has been considered. Along a specified line in y-direction off the antenna, the behaviour of the z-component of  $\vec{E}$  has been compared.

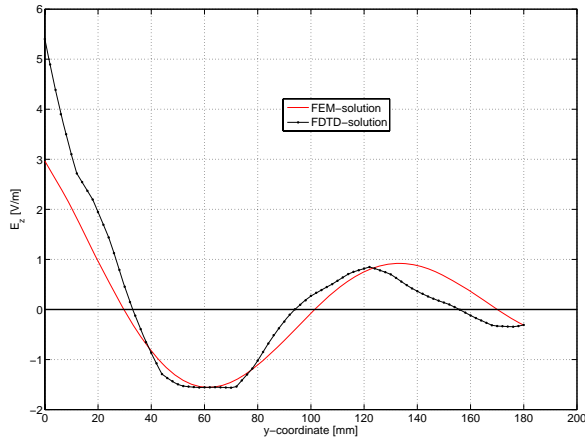


Figure 3: FEM- and FDTD solution of  $E_z$  in comparison.

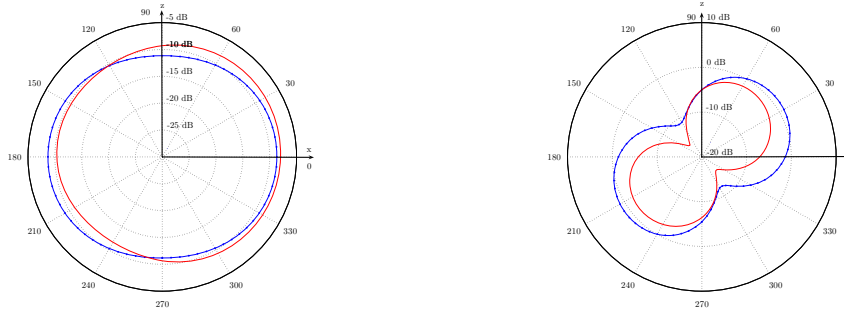
Fig. 3 shows the behavior of  $E_z$  up to the PMLs. Bearing in mind, that the FDTD-procedure works with first order absorbing boundary conditions a sufficient agreement can be observed. This points at an effectual attenuation of the incident wave within the PMLs in the FEM-model.

## B. Metallic side panel and antenna

Subsequently, the USB-antenna with the metallic side panel has been computed. The comparison of this solution with the free space radiating solution is shown below. Therein, the point-marked curve represents the free space solution and the solid curve implies the solution with the side panel.

The diagrams in Fig. 4(a) indicate a non-significant variation in the pattern of  $D_\Phi$ . In case the side panel is present, the radiation characteristic diverges only slightly from the primary one. A more rigorous change can be observed for  $D_\Theta$  in Fig. 4(b). Nearly in all directions a significant decay in the radiation appears.

One should keep in mind, that the magnitude of the  $\Phi$ -component of the  $\vec{E}$ -field is about 10 dB smaller compared with the  $\Theta$ -component.



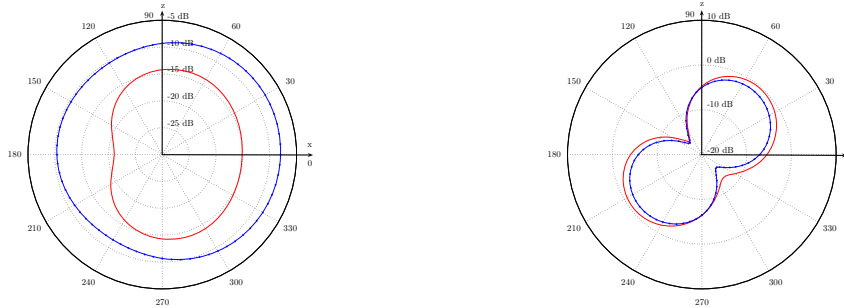
(a) Directivity,  $D_\Phi$  in the  $xz$ -plane.

(b) Directivity,  $D_\Theta$  in the  $xz$ -plane.

Figure 4: Metallic side panel non-coated.

### C. Plastics coated metallic side panel

In the following, the deviation of the radiation pattern for a plastics coated side panel has been investigated. For the computation the plastics coating has been modeled as a layer of 2.0 mm of thickness with a relative permittivity of  $\epsilon_r = 3$ . To show the impact of the layer explicitly, the results have been compared with the non-coated side panel patterns.



(a) Directivity,  $D_\Phi$  in the  $xz$ -plane.

(b) Directivity,  $D_\Theta$  in the  $xz$ -plane.

Figure 5: Metallic side panel plastics-coated.

The non-coated results correspond to the point-marked curves. As can be seen in Fig. 5(a), a high deviation in the directivity of  $D_\Phi$  is evident. The characteristic of the curves changes from a more or less circular loop to a kidney like shape and the magnitude decreases up to  $-10$  dB.

In opposite to the directivity  $D_\Phi$  a non significant influence of the coating layer on the  $\Theta$ -characteristics is found (Fig. 5(b)).

# Conclusion

Various antenna environment configurations have been investigated. In all cases the directivity of the azimuthal component  $D_{\Phi}$  is of minor magnitude. Nevertheless, the form of the patterns change significantly. Concerning the polar angle component  $D_{\Theta}$ , for both form and magnitude a slight variation has been stated, only. For all configurations a reliable wireless LAN connection applying Bluetooth-technology over the specified coverage for class-II radiators is ensured.

## References

- [1] O. Biro, "Edge element formulations of eddy current problems", *Computer methods in applied mechanics and engineering*, vol. 169, pp. 391-405, 1999.
- [2] I. Bardi et. al., "Parameter Estimation for PML's Used with 3D Finite Element Codes", *IEEE Trans. Magn.*, Mag-34, pp. 2755-2758, 1998.
- [3] K. Simonyi, "Theoretische Elektrotechnik", *Barth-Verlag, Leipzig*, 10. Aufl., 1993, p. 880.
- [4] K. Hollaus et al., "Simulation of Simple Topologies on a PCB by a Frequency and a Time Domain Method", *Proceedings of Joint 9th ICEAA '05 and 11th EESC '05*, ISBN 88-8202-094-0, pp. 893-896.
- [5] G.S. Smith, "An introduction to classical electromagnetic radiation", *Cambridge University Press*, ISBN 0 521 58093, 5th ed., 1997, p. 218 ff.